Imaging defects in graphene and carbon nanotubes with a scanning tunneling microscope

Ph. Lambin[a], H. Amara[a,b], J.C. Charlier[b], and V. Meunier[c]

a. Facultés Universitaires Notre-Dame de la Paix, B5000 Namur, Belgium

b. Université Catholique de Louvain, B1348 Louvain-La-Neuve, Belgium

c. Oak Ridge National Laboratory, Oak Ridge, TN37831, USA

Abstract

While the large amount of experimental STM (scanning tunneling microscopy) data obtained so far on perfect nanotubes is well understood, the identification of topological and non-topological modifications of the hexagonal lattice of a carbon nanotube remains an experimental challenge. Thanks to a simple, though accurate theoretical approach, it is possible to simulate the topographic and spectroscopic signatures of many types of defects in graphene and single-walled nanotubes, and to contribute thereby to their identification from STM and STS (scanning tunneling spectroscopy) observations. Several illustrations are provided in this chapter.

I. INTRODUCTION

Since their discovery in 1991,[1] carbon nanotubes have been the subject of an intense research activity. These cylindrical, hollow graphitic molecules have effectively opened the way to nanotechnology, not only thanks to their potential applications, but also by enabling researchers in various fields to gain experience in controlling the nanoworld. Carbon nanotubes are indeed easily produced by a variety of techniques, they are mechanically and chemically stable, they can be manipulated and contacted to external electrodes.

Carbon nanotubes are cylindrically rolled-up sheets of graphene. A single-walled nanotube (SWNT) is composed of just one such, atomic-thick layer. Due to its almost macroscopic length, a nanotube behaves like a solid. Like any solid, a nanotube has defects. An indication that defects indeed exist in single-wall nanotubes is the fact that their internal cavity can be filled with fullerenes in the so-called peapod form, with such a density that fullerenes must enter the nanotubes through the walls in addition to the open ends. The only way making wall entrance possible is via defects.[2] In the same line of thought, recent quantum-mechanical calculations show that missing atoms (vacancy, di-vacancy, or larger holes produced by harsh oxidation) significantly lower the theoretical mechanical strength of SWNTs to values close to experimental observations.[3]

It is difficult to estimate the concentration of defects present in as-prepared nanotubes and to evaluate the effects of purification and separation treatments. In a recent experiment, Ni atoms were adsorbed by electrochemical treatment on a SWNT.[4] Most likely, the Ni atoms adsorb on defects which are much more reactive than the perfect graphitic part of the tube. These Ni atoms may act as nucleation centers for a subsequent growth of atomic clusters, which readily become visible by microscopy. The authors of that experiment reached the conclusion that the average distance between two defects is 4 μm in good-quality SWNTs. It is of course difficult to identify which type of defects is really probed in such an experiment. The point is that the measured concentration of defects is extremely small. It agrees with the observation that SWNTs behave as ballistic conductors over a few μm.[5]

It has been reported from direct chemical titration that SWNTs produced by pulsed laser ablation contain more than 4% of defective sites *after purification* of the samples by acidic oxidation.[6] Arguments exist in the literature that these defects could be pentagon-heptagon pairs, possibly grouped in Stone-Wales defects, which would provide C=C double

bonds where chemistry and functionalization take place.[2] Controlling the chemistry of carbon nanotubes is an important step for the practical development of many potential applications of these nanomaterials. Most of the reactions available today for chemical modifications of the sidewall of a nanotube originate from graphite chemistry.[7] One of the major difficulties to find new chemical reactions is the characterization of the nanotubes, before and after a chemical treatment or functionalization. If it seems clear that nanotubes with a small diameter are more reactive than the big ones,[8] structural defects are believed to increase considerably the reactivity of the nanotube sidewall.[9]

Defects are difficult to observe directly in a nanotube. Of course, pentagon-heptagon pairs are believed to induce observable structural changes such as tapering[10] or sharp bending.[11]. Even with high-resolution Transmission Electron Microscopy (TEM), it is difficult to image a point defect in a SWNT because the resolution of the microscope is generally not good enough to separate the sp^2-bound C atoms. In addition, the images of the front and back sides of the nanotube form a confused Moiré pattern, except for the two achiral tube geometries. Recently, the optical transform of a high-resolution TEM micrography of a SWNT has been used to filter the image of one face of the nanotube through suitable diffraction spots, avoiding the Moiré effect and allowing the identification of an intra-molecular junction with a pentagon-heptagon pair.[12] Scanning tunneling microscopy is by essence an atomic probe. However, the interpretation of STM data is by far not trivial, because the image is the result of mixing both the atomic and electronic structures of the sample. The tip structure itself is convoluted with the sample, making the image confusing. It is the purpose of this paper to present the state of the art in the identification of atomic defects in a graphene layer, including SWNT.

II. TIGHT-BINDING THEORY OF STM

In this section, a brief description of a tight-binding theory of STM is presented. This model is suitable for application to carbon materials whose band structure around the Fermi level is dominated by π electrons[13]. Generalization of the theory to other structures is straightforward. Let us consider an occupied state α on the tip and an unoccupied state β on the sample and let us introduce at time $t = 0$ a small coupling v between the tip and the sample. First-order time-dependent perturbation theory indicates that the probability for

an electron to move from α to β is, asymptotically for large t

$$P_{\alpha\to\beta}(t) \sim \frac{2\pi}{\hbar} t\, |\langle\alpha|v|\beta\rangle|^2 \delta(E_\beta - E_\alpha). \tag{1}$$

The δ function imposes that the two coupled states lie exactly at the same energy (elastic scattering). The amplitude of the probability is proportional to time; provided there is an external wiring through which electrons can move, a stationary current sets up across the STM gap. The total current is then obtained by the time derivative of the probability amplitude, multiplied by the electron charge, and by summing over all states having the same energy while taking into account the occupation probabilities on both sides of the junction:

$$I = \frac{2\pi e}{\hbar} \int dE\, [f_t(E) - f_s(E)] \sum_{\alpha,\beta} |\langle\alpha|v|\beta\rangle|^2 \delta(E - E_\alpha)\delta(E - E_\beta). \tag{2}$$

This expression is the well-known starting point of all the perturbation theories of elastic tunneling. In tight-binding theory, assuming one orbital per atom (an s orbital on the tip apex, as in Tersoff-Hamann theory[14], and one π orbital on the carbon-based sample), the electronic states of the isolated tip and sample are linear combinations of atomic orbitals (LCAO)

$$|\alpha\rangle = \sum_{i\in t} \chi_i^\alpha |\eta_i\rangle \ , \ |\beta\rangle = \sum_{j\in s} \psi_j^\beta |\theta_j\rangle \ . \tag{3}$$

All that is needed is to insert the LCAO expansions in the matrix element $\langle\alpha|v|\beta\rangle$ to end up with that expression of the STM current valid at 0 K

$$I = (2\pi)^2 \frac{e}{h} \int_{E_F - eV}^{E_F} dE \sum_{i,i'\in t} \sum_{j,j'\in s} v_{ij} v^*_{i'j'} n^t_{ii'}(E - \Delta E_F - eV) n^s_{jj'}(E) \tag{4}$$

where V is the tip–sample bias potential ($e > 0$), the E_F's are the Fermi levels of the separated systems and $\Delta E_F = E_F^t - E_F^s$. The current is a sum over sites of the tip and sample of tight-binding representations of the coupling interaction, $v_{ij} = \langle\chi_i|v|\theta_j\rangle$ (see fig. 1), and the imaginary part of energy-dependent Green function elements G of the isolated tip and sample[15]. For the sample, for instance,

$$n^s_{jj'}(E) = \sum_\beta \psi_j^{\beta *} \delta(E - E_\beta) \psi_{j'}^\beta = (-1/\pi)\ \mathrm{Im}\ G^s_{jj'}(E + i0^+). \tag{5}$$

The diagonal elements of the Green function are easily evaluated by the recursion method[16]. It is also true for non-diagonal elements as long as they can be expressed in

terms of diagonal ones[17]. The application of the above formalism to the case of graphitic structures can be further simplified by considering just the π orbital of the C atoms. The assumed point-like tip is modeled by a single s orbital, with a local density of states $n_{ii}^t(E)$ represented by a Gaussian function having its maximum one eV below the Fermi level. The Slater-Koster coupling $s-\pi$ elements are assumed to decrease exponentially with the separation distance d_{ij} between the coupled atoms (tunneling regime):

$$v_{ij} = V_0\, w_{ij}\, \cos\theta_{ij}\, e^{-d_{ij}\lambda} \tag{6}$$

$$w_{ij} = e^{-a d_{ij}^2} / \sum_{j'} e^{-a d_{ij'}^2}. \tag{7}$$

In these expressions, θ_{ij} is the angle between the π orbital axis and the C atom – tip apex direction, $\lambda = 0.085\,\mathrm{nm}$ and $a = 60\,\mathrm{nm}^{-2}$. The w_{ij} are convergence factors chosen to simulate the narrow channel through which the tunneling current flows[18]. The parameter λ is taken such that the tunneling current, proportional to $|v_{ij}|^2$, decreases by one order of magnitude when the tip is retracted by 0.1 nm.

III. APPLICATIONS TO PERFECT GRAPHITIC STRUCTURES

HOPG (highly-oriented pyrolitic graphite) is a real benchmark in STM microscopy, for atomic resolution can easily be obtained in air. The surprising, but well-known result is that the STM image does not usually reproduce the honeycomb structure of the topmost atomic sheet, but it does reveal the triangular Bravais lattice instead[19]. Everything takes place as if every other atoms were missing in the image (see a computed image of graphite in fig. 2). In fact, the two atoms per surface unit cell are not equivalent. One atom has a neighbor in the layer underneath, whereas the other atom has none. It is precisely the latter atom that protrudes in the STM picture at low bias, because the local density of states on this atom has a peak at the Fermi level, while the former atom, being more coupled to the bulk, does not[20]. The situation is of course different in graphene (a single graphite atomic layer): both atoms in the unit cell are equivalent. All atoms appear the same in the STM image and the honeycomb structure is now clearly reproduced. Those effects are shown in fig. 2, which indicates, in addition, that the STM current is small when the tip apex is located above the center of a honeycomb hexagon. Calculations reveal that the small current is due to destructive interferences of the coupling terms between the tip and the six C atoms. As

a result, the hexagon centers in graphene look like corrugation holes in the STM image.

Computed constant-current STM images of three perfect metallic nanotubes are compared in fig. 3. An armchair (10,10) nanotube is shown at the bottom of the drawing. Its image clearly reveals the curved honeycomb network. As in graphene, the corrugation holes where the tip gets closer to the nanotube to keep the current constant are located at the center of the hexagons. In the zigzag (18,0) nanotube depicted at the top of fig. 3, the six-fold symmetry is obviously destroyed: the C-C bonds that are parallel to the tube axis look brighter than the other ones. The origin of this apparent bond anisotropy is geometric[21] and not electronic as with semiconducting tubes (see below). The image of the chiral (13,7) nanotube is somewhat intermediate between those obtained with the armchair and zigzag geometries: the strongest bonds form stripes that spiral around the structure. STM image contrast dominated by stripped features is often observed experimentally with single-walled nanotubes[22].

The case of semiconducting nanotubes is more complex. In the absence of doping – including charge transfer from the substrate that holds the nanotube – one has to apply a bias potential at least equal to half the band gap to probe the conduction band of the sample (negative tip) or its valence band (positive tip). Fig. 3 shows that stripped features in the image of the (13,6) nanotube draw left-handed or right-handed helices around the tube, depending on the potential sign, an effect that has been observed experimentally[23]. Moving from (13,6) to (14,6) reverses the handedness of the strip spirals. In fact, these two nanotubes belong to two different families: those where the difference $n-m$ between the two wrapping indices is a multiple of three *plus* one and those for which $n-m$ is a multiple of three *minus* one. The computed STM image of a semiconducting nanotube strongly depends on the sign of the bias potential[24], unlike the case of metallic tubes, because the symmetries of the HOMO and LUMO wavefunctions are different. For semiconducting nanotubes, the stripped pattern is made by the bonds that have a bonding character. In the above formalism, this means a positive value of the non-diagonal elements $n_{j,j'}(E)$ corresponding to the first-neighbor atoms j and j' of the nanotube.[25] It is not difficult to realize that these elements are odd functions of the energy E relative to the Fermi level. Moving from the conduction band closest to the Fermi level to the valence band symmetrically located below the Fermi level transforms a bonding bond into an antibonding one and *vice versa*.

It is interesting to remark from fig. 3 that there is a distortion in the computed images

of the perfect nanotubes. The structure looks indeed stretched in the horizontal direction perpendicular to the axis. The origin of this phenomena, often observed experimentally[26], is that the STM current "flows" radially between the nanotube and the tip apex, along a path where the tunneling barrier is the shortest.[18,27] As a consequence, the imaged atoms are not right below the apex tip but are located aside from its projection in the horizontal plane[13]. Since the image is recorded as a function of the coordinates of the tip, it is distorted.

IV. DEFECTS IN GRAPHENE

Starting with the simple case of graphene, the STM signature of topological and non-topological modifications of the hexagonal lattice were studied. All the defected structures were optimized by performing first *ab-initio* calculations using the ABINIT code[28]. A supercell representation was used in all calculations. A (5×5) grid, with periodic boundary conditions, was proved to be sufficient to minimize boundary effects on the energy bands of interest. The *ab-initio* results were then reproduced by a tight-binding Hamiltonian incorporating the $2s$ and $2p$ electrons of carbon atoms. The atomic energy levels of the C atoms present around the defect were adjusted together with second-neighbor interactions between two-coordinated atoms, when present, to reproduce the band structure around the Fermi level. These parameters were used for the STM image calculations depicted below. As for the perfect structures of the previous section, only π electrons, which dominate the electronic structure near the Fermi level, were taken into account for the STM calculations.

For the atomic vacancy in graphene, two structures have been reported: the non-reconstructed vacancy, that preserves the D_{3h} symmetry of the honeycomb network, and the reconstructed vacancy with C_s symmetry[29]. The energy of the latter configuration is 0.23 eV lower than the non-reconstructed one (ABINIT result). As shown in fig. 4, the computed STM image of the non-reconstructed vacancy has a large protrusion in the form of a hillock with trigonal symmetry at the center of the defect, which is due to localized electronic states induced by the three dangling bonds. The image also reveals electron-density oscillations resulting from interferences of Fermi waves elastically backscattered by the defect, a feature frequently observed by STM in irradiated graphite. Experimental STM images of graphite indeed show defects in the form of protrusions with trigonal symmetry and, often, a $\sqrt{3} \times \sqrt{3}$ periodic superstructure away from them[30]. Recent experiments, however, have

demonstrated that this superstructure, when present, is induced by an interstitial atom (in between two layers in graphite) but it is absent when there is a vacancy[31]. This finding agrees with the present calculation for graphene, where there is clearly no periodic superstructure in the computed images. However, the horizontal extension and the height of the hillock in the calculated STM image are by far much smaller than observed experimentally. The reason for this discrepancy is unknown. The reconstructed vacancy is even worse in that respect. The STM image of the reconstructed vacancy shown in fig. 4 no longer has a three-fold symmetry. The largest protrusion is located on the sole two-coordinated atom located in front of the pentagon with a long C-C bond produced by the reconstruction. The trigonal symmetry of the image can be restored by invoking a dynamical Jahn-Teller effect[29], where the pentagon rotates by $\pm 2\pi/3$. The image would then be an average of three structures equivalent to that of fig. 4 rotated by $\pm 2\pi/3$.

Another defect of great interest is the di-vacancy, which plays an important role in the conduction properties of SWNTs, as demonstrated recently[32]. A di-vacancy is formed when two neighboring vacancies coalesce. The energy gain with respect to two isolated mono-vacancies is about 6 eV. In a SWNT with small diameter, the formation energy of a di-vacancy can become smaller than that of *one single* mono-vacancy[33]. Fig. 5 shows STM images of a di-vacancy in graphene for opposite tip potentials. There is no dangling bond in the structure. A dumbbell-like feature decorates the two pentagons. Interestingly, the maximum of protrusion is realized right at the center of the defect, where there is no atom. In defect-free graphene, the centers of the hexagons correspond to depressions. Again, contrast oscillations are present around the defect.

The last structural defect we consider is a Stone-Wales $\pi/2$ rotation of a C-C bond which produces two pentagons and two heptagons at the location of four hexagons. Fig. 6 shows the optimized, planar geometry of graphene with such a defect. The STM images, calculated with two opposite bias potentials of the tip, are characterized by an elongated ring of protrusion having its major axis parallel to the Stone-Wales bond and extending from 0.3 to 0.5 nm around the center of the defect. It is clear from the examples above that the defects destroy the atomic resolution of the STM images, although the images were calculated with a point-like tip. Since there is no, or possibly small, buckling of the defected atomic structure in the direction normal to the graphene sheet, all the effects revealed by the STM have an electronic origin. The electron states probed by the tip have a wavelength close

to the Fermi wavelength (0.75 nm), different from the lattice parameter. Since, in addition, there are six equivalent Fermi points, strong interference effects take place, washing out at least locally the apparent periodicity of the atomic structure.

V. DEFECTS IN SINGLE-WALLED CARBON NANOTUBES

We now consider a few defects in SWNTs. Defects have been regularly detected by STM in nanotubes[34] through backscattering electronic effects they may induce.

Stone-Wales defects play probably an important role in the growth process of carbon nanotubes[35]. Most of them can be thermally annealed by back-rotation of the C-C bond, especially in the presence of a C adatom[36]. They can separate in two heptagon-pentagon pairs, which are nothing but dislocations that can further glide along the structure[37], leading to intra-molecular junctions discussed below. Computed STM images of a Stone Wales defect in the common (10,10) nanotube show a perturbation in the form of a ring localized around the defect[38]. There is little effect of the tip bias polarity, unless the voltage is so large that one is probing states below or above the first Van Hove singularity located on each side of the metallic plateau of density of states[39]. The situation is slightly different with semiconducting nanotubes[21]. In any case, the defect strongly affects the image, even 1 nm away from it. As shown in fig. 7 for the particular case of the (10,9) chiral nanotube, the characteristic stripped pattern of the semiconducting tube is washed out in the close neighborhood of the defect. There is a large corrugation hump localized on each pentagon, whose height is 0.15 nm above that of the normal tube. The perturbation brought about by the Stone-Wales defect is weaker and more localized in the case of a positive tip. In both cases, there is nothing in the STM images that presents a five-fold or seven-fold symmetry which could reveal the existence of pentagons and heptagons.

Vacancies in nanotubes can be obtained by ion or electron irradiations or, possibly, by chemical treatment. These defects may be induced on purpose in order to increase the chemical reactivity of a nanotube. It is indeed true that the presence of dangling bonds around a mono-vacancy leads to a peak in the density of states at the Fermi level[40]. This is the reason why computed STM images show a mono-vacancy in a SWNT in the form of a protrusion hillock (see fig. 10), as in graphene, with a linear width of 0.5 nm and a heigh varying between 0.6 nm in metallic nanotubes and 0.3 nm in semiconducting nanotubes.[41]

Many reports exist in the literature on the doping of nanotubes by substituting impurities for carbon atoms. Boron and nitrogen are the most natural atoms to consider for that purpose, since their are located next to C in the periodic table of the elements. With the hypothesis that the perfect sp^2 network is not affected by the hetero-atom, a N substitution impurity induces quasi-bound states located 0.6-0.9 eV above the Fermi level in a (10,10) nanotube (DFT calculations).[42] A nitrogen atom in the C graphitic structure forms a potential well that may be represented in tight-binding by a continuous decrease of the on-site energies by 2.6 eV in the vicinity of the impurity, while keeping constant the $\pi - \pi$ hopping integral (γ_0 = -2.9 eV).[43] The perturbation of the atomic levels brought about by a N impurity, due to charge transfers, extends ~ 0.5 eV away from it. The potential well just mentioned leads to a large quasi-bound state in the valence bands of a semiconductor nanotube. This impurity state in the (14,6) nanotube is revealed by the STM images of fig. 8 for a negative tip (potential measured with respect to the nanotube Fermi level at mid gap) that probe unoccupied states. With $V = -0.4$ and -0.8 eV, high protrusions exist on the N impurity (located right at the origin of the coordinates in the images) and on C atoms around it, up to 0.6 nm. With a positive tip (scanning of the occupied states), the image is very similar to the one of the perfect nanotube (refer to fig. 3). It is interesting to remark that that the N-C bonds are non-bonding in the vicinity of both the HOMO and LUMO states. In the STM images, indeed, there is a local minimum of corrugation at the the center of the three first-neighbor bonds.

The fact the N impurity acts as a donor of electron can be seen directly in fig. 9, which shows a dI/dV STS curve computed 0.6 nm right above the N impurity (full line) compared to the same curve in the perfect (14,6) nanotube (dashed line). The STS curve is strongly asymmetric in the former case compared to the latter: the unoccupied states (positive sample voltage V_s) are clearly enhanced compared to the occupied one on the N impurity.

VI. INTRA-MOLECULAR JUNCTIONS

Intra-molecular junctions, where two half nanotubes with different chiralities are interconnected are interesting objects because when such a structure is recognized, one can be sure that defects are present in the connection region. Again, the atomic resolution is lost in that region, making the identification of the defects difficult[44–46]. An example is pro-

vided by fig. 11 that shows experimental images of an intra-molecular junction between two semiconducting SWNTs.

The possibility of identifying defects in single-walled nanotubes by a combination of STM and STS measurements has been demonstrated recently[46]. Here, a structure resembling the intra-molecular junction between two nanotubes was observed experimentally with an STM. The nanotube segments on both part of the junction have different chiralities, which requires at least one pentagon and one heptagon to interconnect them. Calculations of STM images and STS spectra were performed using a tight-binding theory similar to the one described here above. STM images and STS spectra were calculated for a variety of possible structures and compared to the observations. The best fit of the experimental data favored a connection between two metallic nanotubes, (29,5) and (21,3), with two opposite pentagon-heptagon pairs at the interface. Each defect gives rise to wave interference patterns whose periodicities agree with experiment. This example demonstrates that defects can possibly be identified with STM, despite the fact that the atomic resolution is lost in the vicinity of the defect. However, electronic effects induced by the defect may be so strong and so spatially extended in a nanotube that careful comparisons of the observed STM contrasts with image calculations may serve as resolving the underlying atomic structure unambiguously.

Acknowledgments

This work has been funded by the Belgian state Science Policy Programming Services through the IUAP program P5/01 "Quantum size effects in nanostructured materials". Part of this research was conducted at the Center for Nanophase Materials Sciences, which is sponsored at Oak Ridge National Laboratory by the Division of Scientific User Facilities, U.S. Department of Energy (VM). The authors acknowledge Sylvain Latil for helpful discussions.

---

[1] S. Iijima, Nature **354**, 56 (1991).

[2] M. Monthioux, Carbon **40**, 1809 (2002).

[3] S.L. Mielke, D. Troya, S. Zhang, J.L. Li, S. Xiao, R. Car, R.S. Ruoff, G.C. Schatz, and T. Belytschko, Chem. Phys. Lett. **390**, 413 (2004).

[4] Y. Fan, B.R. Goldsmith, and Ph.G. Collins, Nat. Mat. **4**, 906 (2005).

[5] S.J. Tans, M.H. Devoret, H. Dai, A. Thess, R.E. Smalley, L.J. Geerligs, and C. Dekker, Nature **386**, 474 (1997).

[6] D.B. Mawhinney, V. Naumenko, A. Kuznetsova, J.T. Yates Jr, J. Liu, and R.E. Smalley, Chem. Phys. Lett. **324**, 213 (2000).

[7] J.L. Bahr and J.M. Tour, J. Mater. Chem. **12**, 1952 (2002).

[8] S. Niyogi, M.A. Hamon, H. Hu, B. Zhao, P. Bhowmik, R. Sen, M.E. Itkis, and R.C. Haddon, Acc. Chem. Res. **35**, 1105 (2002).

[9] J.A. Robinson, E.S. Snow, S.C. Badescu, T.L. Reinecke, and F.K. Perkins, Nano Lett. **6**, 1747 (2006).

[10] S. Iijima, T. Ichihashi, and Y. Ando, Nature **356**, 776 (1992).

[11] M. Terrones, W.K. Hsu, J.P. Hare, H.W. Kroto, H. Terrones, and D.R.M. Walton, Phil. Trans. R. Soc. London A **354**, 2025 (1996).

[12] A. Hashimoto, K. Suenaga, A. Gloter, K. Urita, and S. Iijima, Nature **430**, 870 (2004).

[13] V. Meunier and Ph. Lambin, Phys. Rev. Lett. **81**, 5888 (1998).

[14] J. Tersoff and D.R. Hamann, Phys. Rev. Lett. **50**, 1998 (1983).

[15] K. Kobayashi and M. Tsukada, J. Vac. Sci. Technol. A **8**, 170 (1990).

[16] R. Haydock, V. Heine and M.J. Kelly, J. Phys. C Solid St. Phys. **5**, 2845 (1972).

[17] J. Inoue, A. Okada and Y. Ohta, J. Phys.: Condens. Matter **5**, L465 (1995).

[18] G.I. Márk, L.P. Biró, and J. Gyulai, Phys. Rev. B **58**, 12645 (1998).

[19] H.J. Guntherodt and R. Wiesendanger (eds.), "Scanning tunneling microscopy I" (Springer-Verlag Berlin 1994), p. 136-179.

[20] D. Tománek and S.G. Louie, Phys. Rev. B **37**, 8327 (1988).

[21] V. Meunier and Ph. Lambin, Phil. Trans. R. Soc. Lond. A **362**, 2187 (2004).

[22] W. Clauss, Appl. Phys. A **69**, 275 (1999).

[23] W. Clauss, D.J. Bergeron, M. Freitag, C.L. Kane, E.J. Mele, and A.T. Johnson, Europhys. Lett. **47**, 601 (1999).

[24] C.L. Kane and E.J. Mele, Phys. Rev. B **59**, R12759 (1999).

[25] V. Meunier, P. Senet, and Ph. Lambin, Phys. Rev. B **60**, 7792 (1999).

[26] L.C. Venema, V. Meunier, Ph. Lambin, and C. Dekker, Phys. Rev. B **61**, 2991 (2000).

[27] M. Ge and K. Sattler, Appl. Phys. Lett. **65**, 2284 (1994).

[28] X. Gonze, J.M. Beuken, R. Caracas, F. Detraux, M. Fuchs, G.M. Rignanese, L. Sindic, M.

Verstraete, G. Zerah, F. Jollet, M. Torrent, A. Roy, M. Mikami, Ph. Gosez, J.Y. Raty, and D. C. Allan, Comput. Mat. Sc. **25**, 478 (2002).

[29] A.A. El-Barbary, R.H. Telling, C.P. Ewels, M.I. Heggie, and P.R. Briddon, Phys. Rev. B **68**, 144107.1 (2003).

[30] J. Valenzuela-Benavides and L. Morales de la Garza, Surf. Sci. **330**, 227 (1995).

[31] J.R. Hahn and H. Kang, Phys. Rev. B **60**, 2007 (1999).

[32] C. Gómez-Navarro, P. J. De Pablo, J. Gómez-Herrero, B. Biel, F. J. Garcia-Vidal, A. Rubio and F. Flores, Nature Mater. 4 , 534 (2005).

[33] A.V. Krasheninnikov, P.O. Lehtinen, A.S. Foster, and R.M. Nieminen, Chem. Phys. Lett. **418**, 132 (2006).

[34] T.M. Odom, J.L. Huang, and C.M. Lieber, J. Phys.: Condens. Matter **14**, R145 (2002).

[35] J.C Charlier and S. Iijima, in *Carbon Nanotubes: Synthesis, Structure, Properties and Application*, M. S. Dresselhaus, G. Dresselhaus, and Ph. Avouris (Eds.) (Springer, Berlin, 2001), 55.

[36] C.P. Ewels, M.I. Heggie, and P.R. Briddon, Chem. Phys. Lett. **351**, 178 (2002).

[37] M. Buongiorno Nardelli, B.I. Yakobson, and J. Bernholc, Phys. Rev. B **57**, R4277 (1998).

[38] D. Orlikowski, M. Buongiorno Nardelli, J. Bernholc, and Ch. Roland, Phys. Rev. B **61**, 14194 (2000).

[39] Y. Miyamoto, A. Rubio, S. Berber, M. Yoon, and D. Tománek, Phys. Rev. B **69**, 121413R.1 (2004).

[40] L. Chico, L.X. Benedict, S.G. Louie, and M.L. Cohen, Phys. Rev. B **54**, 2600 (1996).

[41] A.V. Krasheninnkov, Sol. St. Commun. **118**, 361 (2001).

[42] H.J. Choi, J. Ihm, S.G. Louie, and M.L. Cohen, Phys. Rev. Lett. **84**, 2917 (2000).

[43] Ch. Adessi, Stephan Roche, and X. Blase, Phys. Rev. B **73**, 125414.1 (2006).

[44] M. Ouyang, J.L. Huang, and Ch.M. Lieber, Science **291**, 97 (2001).

[45] H. Kim, J. Lee, S.J. Kahng, Y.W. Son, S. B. Lee, C.K. Lee, J. Ihm, and Young Kuk, Phys. Rev. Lett. **90**, 216107.1 (2003).

[46] M. Ishigami, H.J. Choi, S. Aloni, S.G. Louie, M.L. Cohen, and A. Zettl, Phys. Rev. Lett. **93**, 196803.1 (2004).

Figure caption

1. Left: schematic model of the STM junction between a tip (t) and a sample (s). Right: Tight-binding coupling between atomic sites on both sides of the STM junction.

2. Constant-height STM current map calculated 0.5 nm above graphite (top) and above a single graphene sheet (bottom). The tight-binding calculations for graphite were performed with two coupled graphene sheets in the Bernal arrangement. Here and in subsequent 2D representations of STM images, all coordinates are expressed in Å.

3. Computed constant-current STM images of three metallic nanotubes with tip potential $V = 0.1\,\mathrm{V}$ (top) and two semiconducting nanotubes for two opposite bias potential of the tip (0.4 V, bottom).

4. Computed constant-current STM images of a mono-vacancy in graphene calculated with a positive tip potential (0.2 V): non-reconstructed D_{3h} (top) and reconstructed C_s (bottom) structures.

5. Computed constant-current STM images of a di-vacancy in graphene, calculated with a negative ($-0.2\,\mathrm{V}$, top) and positive ($+0.2\,\mathrm{V}$, bottom) tip potential.

6. Computed constant-current STM images of a Stone-Wales defect in graphene, calculated with a negative ($-0.2\,\mathrm{V}$, top) and positive ($+0.2\,\mathrm{V}$, bottom) tip potential.

7. Computed constant-current STM images of a Stone-Wales defect in the (10,9) nanotube, calculated with a negative ($-0.4\,\mathrm{V}$, top) and positive ($+0.4\,\mathrm{V}$, bottom) tip potential. The structure was optimized in tight binding. This figure, like the following, represents the height of the tip in Å measured from the axis of the nanotube along the radial direction. In this way, the geometric corrugation due to the curvature of the nanotube is discarded.

8. Computed constant-current STM images of (14,6) nanotube with a N substitution impurity located at the center of images. Three bias potential of the tip have been considered: -0.8 (top), -0.4 (middle) and $+0.4\,\mathrm{V}$ (bottom).

9. STS dI/dV spectrum computed 6 nm above a N substitution impurity in (14,6) nanotube (full line) and for a perfect (14,6) nanotube (dashed line) as a function of the

sample bias potential V_s.

10. Tight-binding computed STM image, after filtering, of a mono-vacancy in the semiconductor (14,0) zig-zag nanotube for tip potential (a) $+0.4\,\mathrm{V}$ and (b) $-0.4\,\mathrm{V}$. The asymmetry between the two images comes from the fact that the Fermi level of the nanotube was placed near the top of the valence band. Occupied states are probed in (a) whereas in (b), localized gap states induced by the dangling bonds are probed. Reproduced with permission from ref. 41, A.V. Krasheninnkov, Sol. St. Commun. 118, 361 (2001). Copyright 2001 Elsevier.

11. Experimental STM images of an intra-molecular junction between two semiconducting nanotubes – possibly (15,2) (left) and (19,3) (right) – for tip potentials (b) -1.5, (c) -0.5, and (d) $0.3\,\mathrm{V}$. Reproduced with permission from ref. 45, H. Kim *et al*, Phys. Rev. Lett. 90, 216107 (2003). Copyright 2003 American Physical Society.

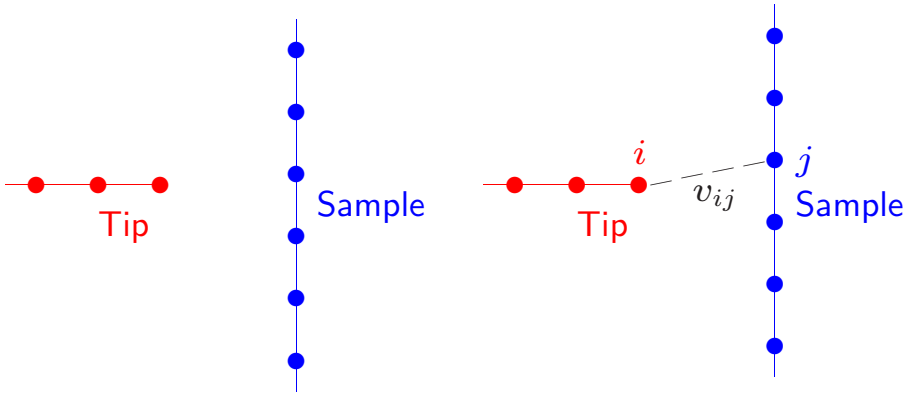

FIG. 1: Left: schematic model of the STM junction between a tip (t) and a sample (s). Right: Tight-binding coupling between atomic sites on both sides of the STM junction.

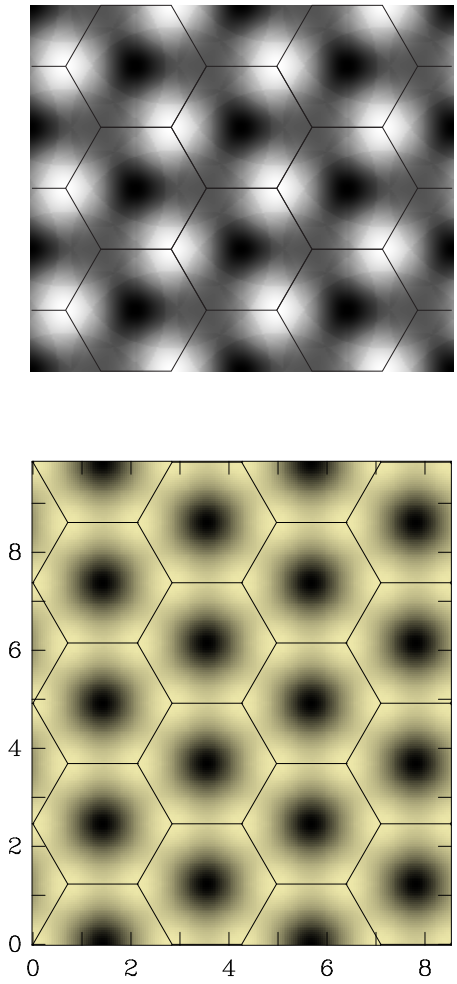

FIG. 2: Constant-height STM current map calculated 0.5 nm above graphite (top) and above a single graphene sheet (bottom). The tight-binding calculations for graphite were performed with two coupled graphene sheets in the Bernal arrangement. Here and in subsequent 2D representations of STM images, all coordinates are expressed in Å.

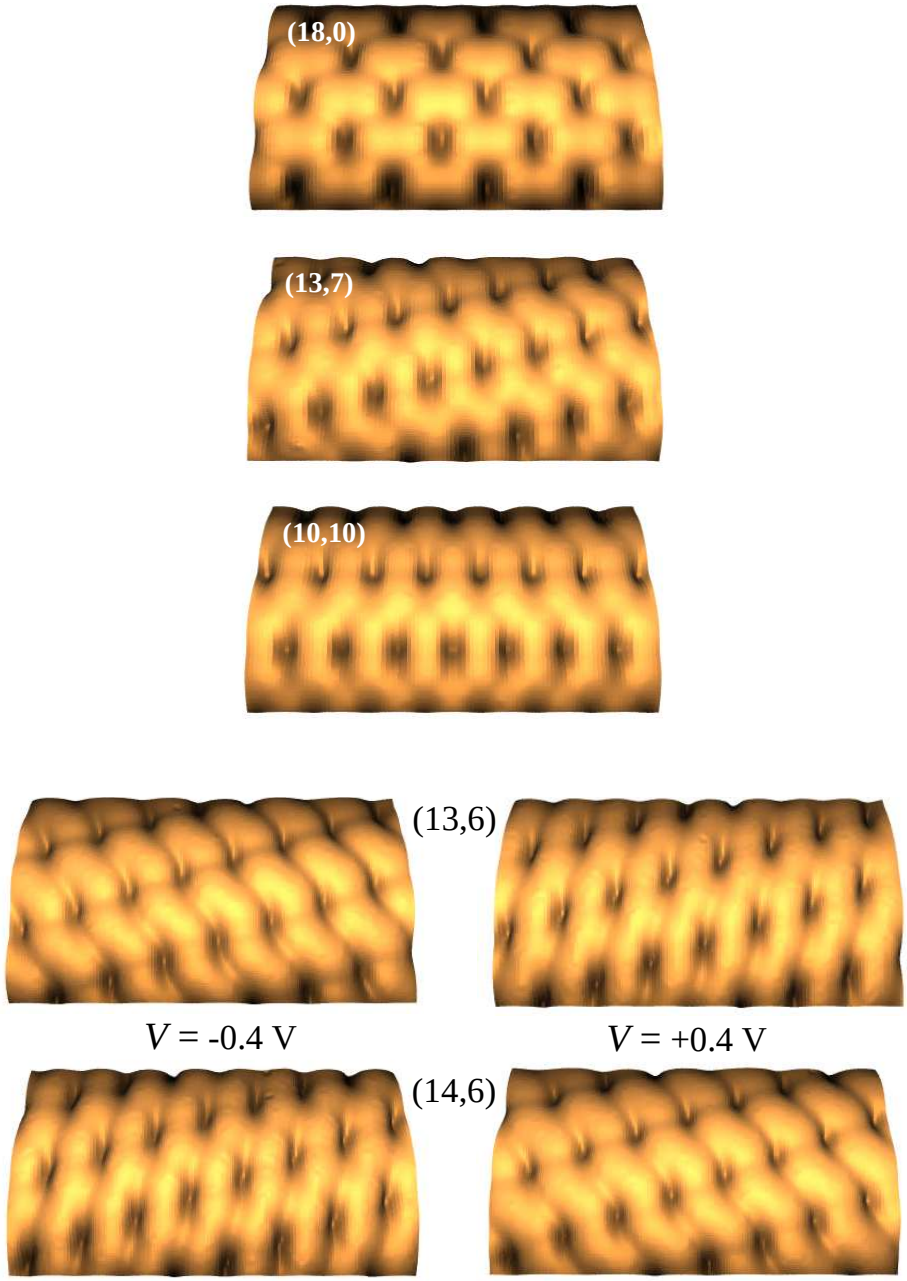

FIG. 3: Computed constant-current STM images of three metallic nanotubes with tip potential $V = 0.1\,\mathrm{V}$ (top) and two semiconducting nanotubes for two opposite bias potential of the tip (0.4 V, bottom).

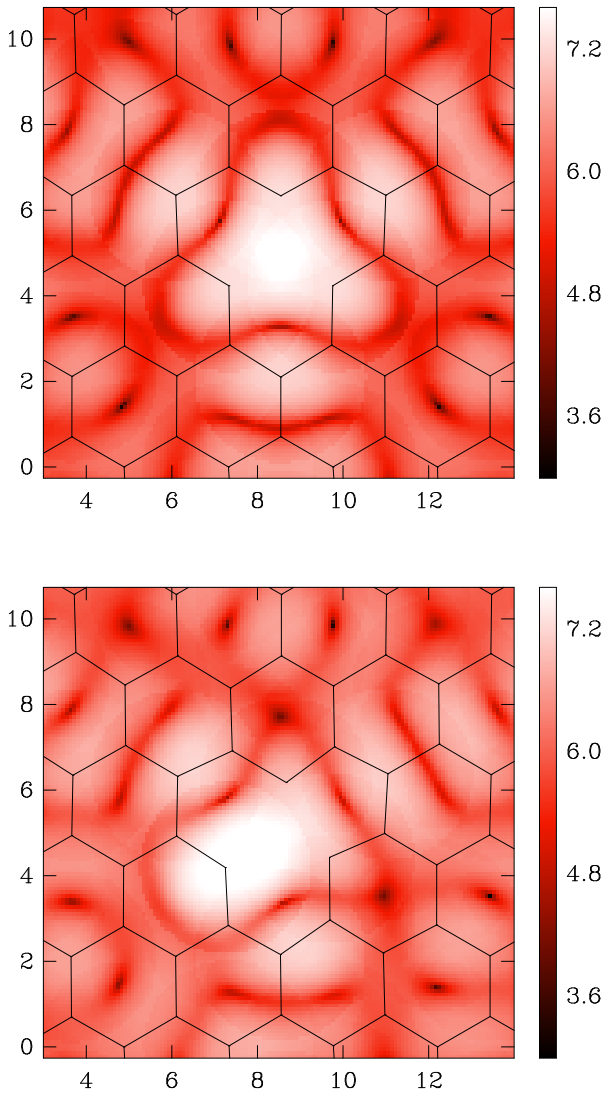

FIG. 4: Computed constant-current STM images of a mono-vacancy in graphene calculated with a positive tip potential (0.2 V): non-reconstructed D_{3h} (top) and reconstructed C_s (bottom) structures.

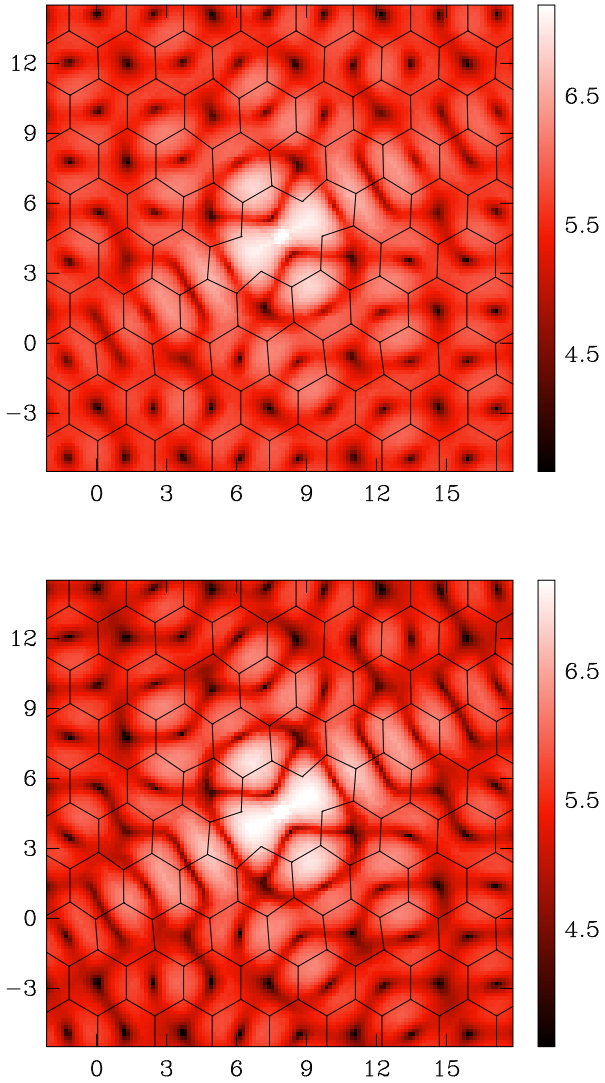

FIG. 5: Computed constant-current STM images of a di-vacancy in graphene, calculated with a negative (−0.2 V, top) and positive (+0.2 V, bottom) tip potential.

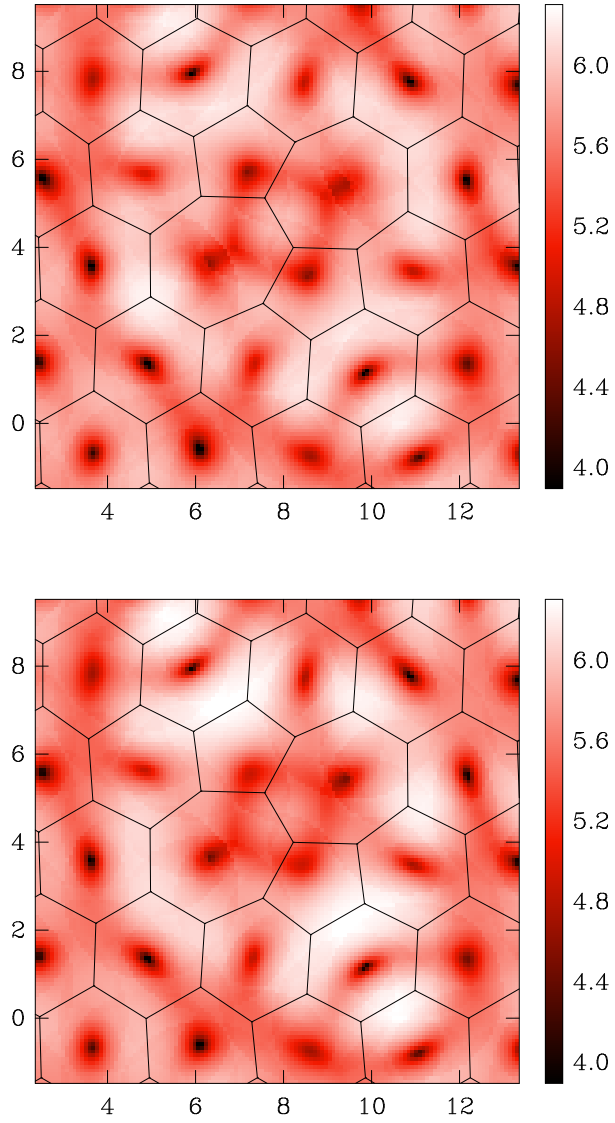

FIG. 6: Computed constant-current STM images of a Stone-Wales defect in graphene, calculated with a negative ($-0.2\,\mathrm{V}$, top) and positive ($+0.2\,\mathrm{V}$, bottom) tip potential.

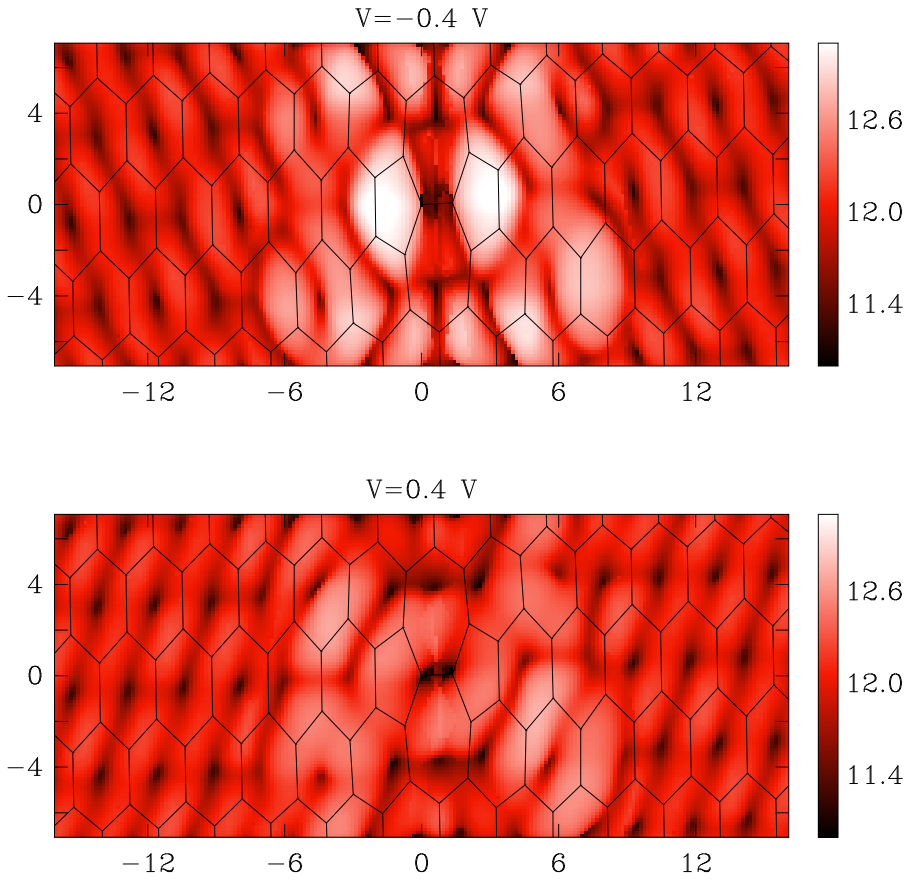

FIG. 7: Computed constant-current STM images of a Stone-Wales defect in the (10,9) nanotube, calculated with a negative (−0.4 V, top) and positive (+0.4 V, bottom) tip potential. The structure was optimized in tight binding. This figure, like the following, represents the height of the tip in Å measured from the axis of the nanotube along the radial direction. In this way, the geometric corrugation due to the curvature of the nanotube is discarded.

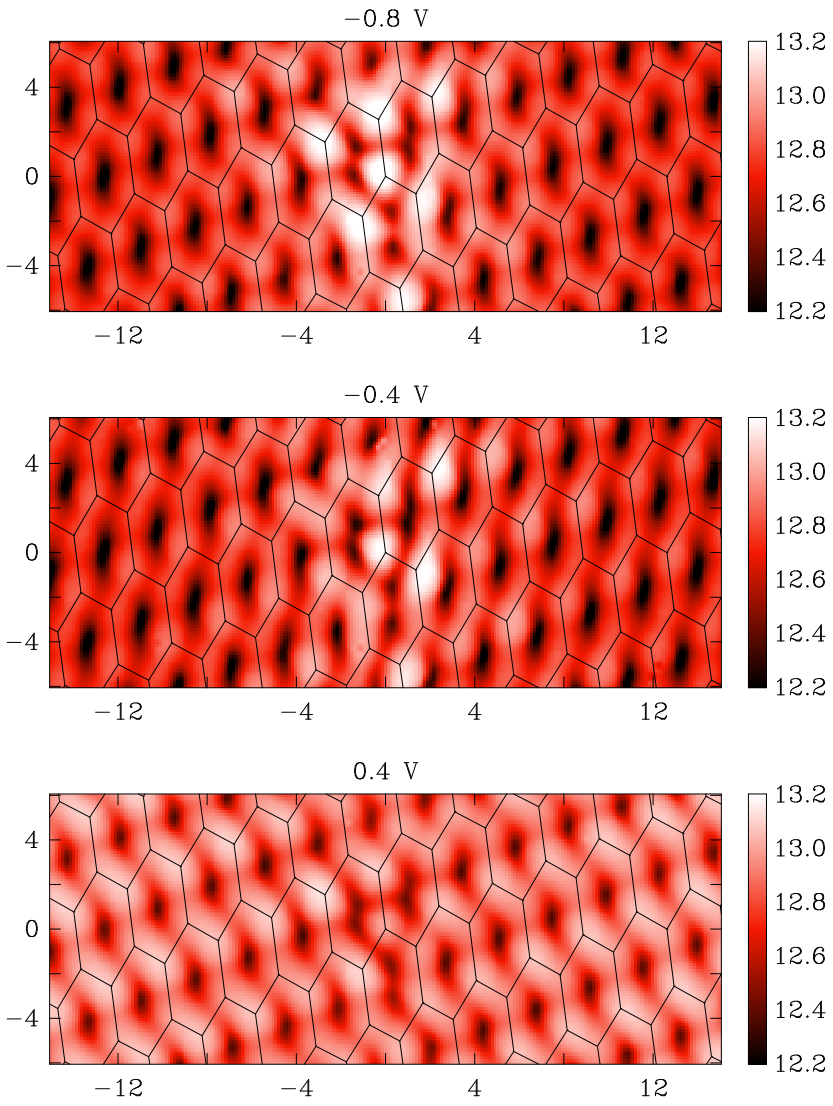

FIG. 8: Computed constant-current STM images of (14,6) nanotube with a N substitution impurity located at the center of images. Three bias potential of the tip have been considered: −0.8 (top), −0.4 (middle) and +0.4 V (bottom).

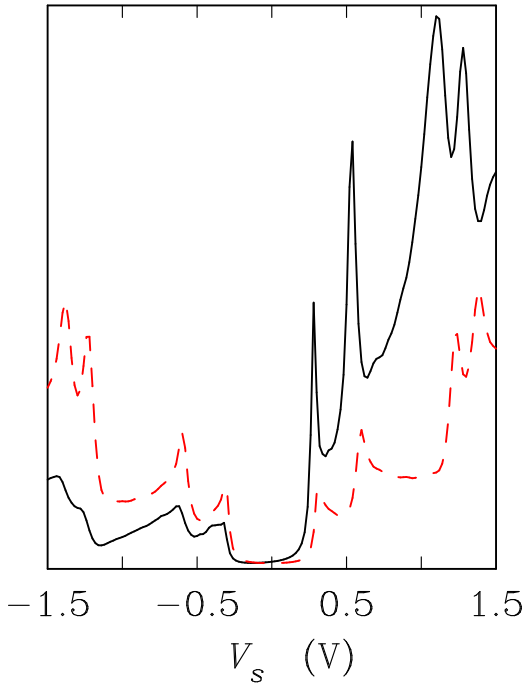

FIG. 9: STS dI/dV spectrum computed 6 nm above a N substitution impurity in (14,6) nanotube (full line) and for a perfect (14,6) nanotube (dashed line) as a function of the *sample* bias potential V_s.

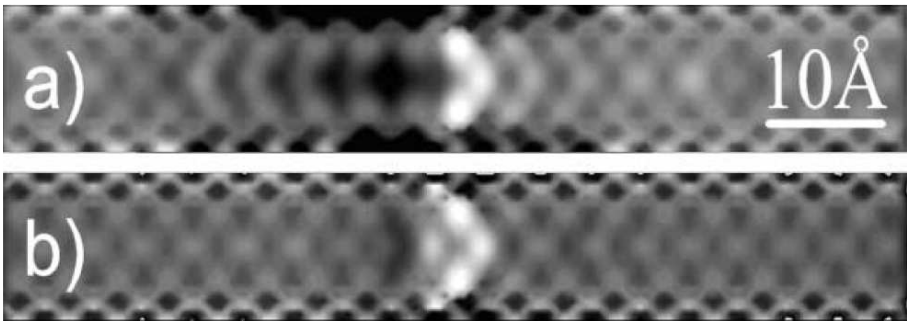

FIG. 10: Tight-binding computed STM image, after filtering, of a mono-vacancy in the semiconductor (14,0) zig-zag nanotube for tip potential (a) $+0.4\,\mathrm{V}$ and (b) $-0.4\,\mathrm{V}$. The asymmetry between the two images comes from the fact that the Fermi level of the nanotube was placed near the top of the valence band. Occupied states are probed in (a) whereas in (b), localized gap states induced by the dangling bonds are probed. Reproduced with permission from ref. 41, A.V. Krasheninnkov, Sol. St. Commun. 118, 361 (2001). Copyright 2001 Elsevier.

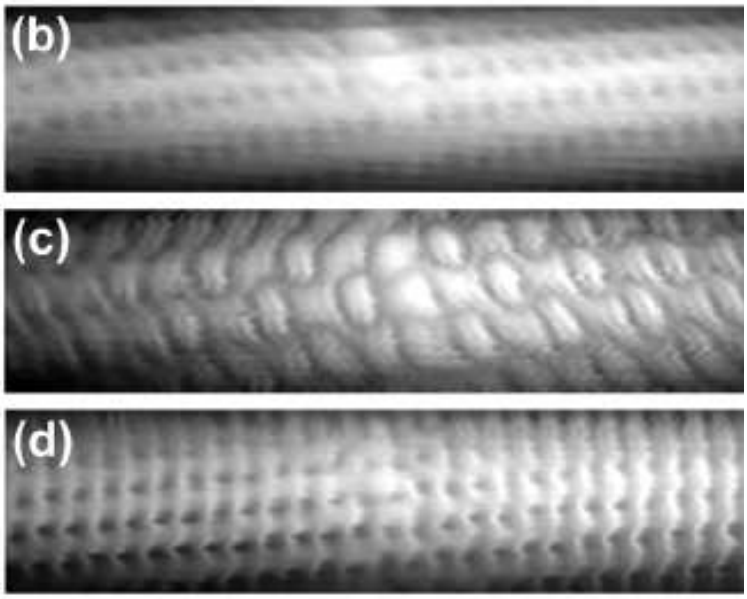

FIG. 11: Experimental STM images of an intra-molecular junction between two semiconducting nanotubes – possibly (15,2) (left) and (19,3) (right) – for tip potentials (b) -1.5, (c) -0.5, and (d) 0.3 V. Reproduced with permission from ref. 45, H. Kim *et al*, Phys. Rev. Lett. 90, 216107 (2003). Copyright 2003 American Physical Society.